Korean Journal of Chemical Engineering (2024) 41:2059–2067
https://doi.org/10.1007/s11814-024-00134-0

ORIGINAL ARTICLE

Microbial Treatment of Azo Dyes Using Biogenic Bimetallic Iron–Molybdenum Nanoparticles

Sun-Wook Jeong[1] · Jung Eun Yang[2] · Yong Jun Choi[1]

Received: 15 December 2023 / Revised: 20 January 2024 / Accepted: 6 February 2024 / Published online: 12 February 2024
© The Author(s), under exclusive licence to Korean Institute of Chemical Engineers, Seoul, Korea 2024

Abstract

Azo compounds have long posed a serious threat to publish health and the aquatic environment. Therefore, the adverse effects of azo compounds on public health have inspired the need to develop efficient and reliable treatment methods. Although various physicochemical treatment methods have been developed, bio-inspired environmentally friendly treatment method have not yet been reported. Here, we report the development of a novel azo compound treatment method using biogenic nanoparticles immobilized microorganism. Firstly, biogenic bimetallic iron–molybdenum nanoparticles immobilized *Deinococcus radiodurans* R1 (DR-FeMoNPs) were constructed. Next, physicochemical properties of FeMoNPs including specific surface area (53.627 $m^2\ g^{-1}$), pore volume (0.3561 $cm^3\ g^{-1}$), and average pore diameter (19.205 nm) were thoroughly addressed. The resulting FeMoNPs-immobilized *D. radiodurans* R1 exhibited an 87.2% removal efficiency for Congo Red, with a maximum capacity of 172.4 mg/g. Additionally, the rapid degradation of residual H_2O_2, triggering Fenton-like reaction via biological scavenging mechanism, was confirmed. DR-FeMoNPs also demonstrated highly efficient removal of other types of azo compounds, such as Acid Orange 7 (99.4%) and Evans Blue (81.1%).

Keywords Bioremediation · Fenton reaction · Nanomaterials · Microorganism · Azo compounds

Introduction

Azo dyes, which are organic compounds containing colored azo functional groups (*N*=*N*-), are widely used in the dyeing industry but exhibit carcinogenic and mutagenic activity when exposed to the human body [1, 2]. Thus, over the past decades, particular attention has been focused on the development of efficient and stable methods for treating dye wastewater through physicochemical methods, such as adsorption, ion exchange, chemical oxidation, and membrane processes [3–5].

The Fenton reaction, an advanced oxidation process, is widely used to treat toxic azo dyes using iron-based nanoparticles in contaminated water [1]. For example, 200 mg/g of maximum removal capacity and 95.6% of degradation efficiency of Direct Red 23 were successfully achieved using a Co-Fe hydrotalcite-mediated Fenton reaction [6]. A modified Fenton-like reaction method using magnetic iron (II, III) oxide-manganese (IV) oxide (Fe_3O_4-MnO_2) core–shell nanoplates which was also developed to treat Acid Orange 7 contaminated water [7]. Although these methods have demonstrated remarkable performance in processing azo dyes, several drawbacks still need to be addressed. As the Fenton reaction is highly pH dependent reaction, the pH value must be maintained in acidic pH condition (pH 3.5 ~ pH 5.5) where the iron is existed in a ferrous form (Fe^{2+}) [8]. In addition, the Fenton reaction not only requires high energy to maintain the necessary reaction conditions, such as temperature and pH, but also raises potential safety issues due to the use of high concentration of H_2O_2 [9, 10]. These drawbacks have commonly occurred in various physicochemical methods for the treatment of toxic pollutants.

To address the shortcomings encountered in conventional physicochemical treatment methods, green synthesis

Sun-Wook Jeong and Jung Eun Yang have contributed equally to this work.

✉ Yong Jun Choi
yongjun2165@uos.ac.kr

[1] School of Environmental Engineering, University of Seoul, Seoul 02504, Republic of Korea

[2] Department of Advanced Process Technology and Fermentation, World Institute of Kimchi, Gwangju 61755, Republic of Korea

technology, which involves the bio-based synthesis of nanoparticles, has emerged as a promising method to compensate for the limitations of traditional approaches. Recently, a novel bioremediation method for the treatment of radioactive iodine (> 99%) was developed using biogenic gold nanoparticles containing extremophilic microorganism, *Deinococcus radiodurans* R1 strain [11]. Another study also reported a highly efficient and stable method for removing toxic arsenic was also developed using magnetic iron nanoparticles immobilized *D. radiodurans* R1 strain [12]. These methods improve the removal efficiency of various toxic pollutants through the immobilization of nanoparticles synthesized by microorganisms. It has the potential not only for environmentally friendly biosynthesis of nanoparticles but also for overcome the limitations of existing physicochemical process.

These observations compelled us to develop a highly efficient treatment method for the removal of toxic azo compounds through the combination of the toughest microorganism and the green synthesis of nanomaterials. This method was successfully achieved using *D. radiodurans* R1 immobilized with biogenic bimetallic iron–molybdenum nanoparticles (DR-FeMoNPs). The DR-FeMoNPs showed remarkable efficiency in the treatment of Congo Red (up to 87.2%), Acid Orange 7 (up to 99.4%), and Evans Blue (up to 81.1%). Furthermore, the H_2O_2 remaining after the Fenton reaction was rapidly removed through a biological scavenging process.

Materials and Methods

Preparation of Biogenic *D. radiodurans* Iron–Molybdenum Nanoparticles

The *D. radiodurans* R1 (ATCC13939) cells were used for the FeMoNP biosynthesis and the control (without biosynthesis) in all tests. The cells were routinely cultivated in a TGY (0.5% tryptone, 0.1% glucose, and 0.3% yeast extract) medium at 30 °C with agitation. Moreover, *D. radiodurans* R1 was cultured in 50 mL of liquid TGY medium until $OD_{600} = 1$ and was used to synthesize the FeMoNPs. Next, 9.389 mM of $Na_2MoO_4 \cdot 2H_2O$ (Duksan, Korea) and 6.5 mM of $FeCl_3 \cdot 6H_2O$ (Samchun, Korea) were added to the cell cultures, which were further incubated for 24 h at 30 °C. The mixtures were centrifuged at 15,982 × *g* for 5 min, and the resulting pellets were rinsed twice with deionized water to remove the partly immobilized FeMoNPs on the cell surface.

Cell Viability Test

The cell viability of *D. radiodurans* R1 after completing the nanoparticle fabrication or Fenton-like reaction was evaluated via plating assays. The samples were rinsed twice with deionized water to remove residual metal ions or H_2O_2 from the cells. Afterward, the samples were resuspended in 1 mL of liquid TGY medium, and the suspensions were serially diluted and spotted onto TGY agar plates.

Characterization of the Biogenic Iron–Molybdenum Nanoparticles

The morphology and elemental composition of the FeMoNPs were determined via scanning electron microscopy (SEM) energy-dispersive X-ray spectrometry (EDX; SU8010, Hitachi, Japan), as previously described [12]. Briefly, *D. radiodurans* iron–molybdenum nanoparticles (DR-FeMoNPs) were fixed in 2.5% glutaraldehyde solution and dehydrated in a series with ethanol (30%, 50%, 60%, 70%, 80%, 90%, and 99%). The size distribution of the FeMoNPs was determined using dynamic light scattering (DLS) analysis with a Zetasizer Nano ZS (Malvern Instruments, UK). For this purpose, the FeMoNPs were separated from the *D. radiodurans* R1 cells by beating (4,032 × *g*, 3 min) using a FastPrep-24 instrument (MP Biomedicals, Korea). The separated FeMoNPs were rinsed twice with deionized water and used in further tests.

The crystallographic structure was determined via X-ray diffraction (XRD, SmartLab, Rigaku, Japan) with 2θ angles from 5° to 70° and a sweep speed of $4°min^{-1}$. The surface composition of the purified FeMoNPs was determined using X-ray photoelectron spectroscopy (XPS) with a K-Alpha plus X-ray photoelectron spectrophotometer (Thermo Fisher Scientific, Waltham, MA, USA) equipped with monochromatic Al Kα ($h\nu = 1486.7$ eV) radiation. The specific surface areas and pore sizes of the FeMoNPs were measured using a BELSORP-mini X (Soletek, Korea) with the Brunauer–Emmett–Teller (BET) and Barrett–Joyner–Halenda (BJH) methods, respectively.

Treatment of Azo Dyes Using *D. radiodurans* Iron–Molybdenum Nanoparticles

The degradation of Congo Red in an aqueous solution by the DR-FeMoNPs was performed in a batch and carried out in the dark at room temperature. The concentration of Congo Red was determined by measuring the absorbance at a wavelength of 498 nm, using an Epoch microplate ultraviolet–visible (UV–Vis) spectrophotometer (BioTek, Winooski, VT, USA). The sample (1 mg) was placed in 1 mL of Congo Red solution with an initial concentration of 200 mg/L. The H_2O_2 solution (0.2 M) was immediately added to initiate a Fenton-like reaction. The Congo Red concentration after H_2O_2 treatment was measured during 3 h. Different concentrations of Congo Red, ranging from 50 to 300 mg/L, were tested to determine the optimal conditions for Congo Red

degradation by DR-FeMoNPs. Moreover, different concentrations of H_2O_2 ranging from 0.001 to 3 M were added to the DR-FeMoNP and Congo red mixtures. At the end of the reaction, the mixtures were centrifuged at 15,982 × *g* for 5 min. The degradation efficiency (%) and capacity (mg/g) were calculated according to the following equations:

$$\text{Degradation efficiency (\%)} = \frac{C_0 - C_t}{C_0} \times 100 \quad (1)$$

$$\text{Degradation capacity (mg/g)} = \frac{C_0 - C_t}{X} \quad (2)$$

where C_t and C_0 are the dye concentrations initially and at time t (min), respectively, and X is the biomass amount (mg/L) used to test the dye degradation. The degradation efficiency of Acid Orange 7 and Evans Blue (100 mg/L of initial concentration) was also evaluated by measuring the absorbance at wavelengths of 484 nm and 608 nm, respectively. The H_2O_2 concentration was measured by the colorimetric quantification method, using 1% titanium sulfate as previously described [13]. The maximum adsorption peaks were measured at 400 nm using a UV–Vis spectrophotometer (Epoch, USA).

Metal Leaching

The final concentration of 0.2 M H_2O_2 was added to 50 mL of the reaction mixture containing 1 g/L DR-FeMoNPs and 100 mg/L Congo red for 3 h at room temperature. The supernatants were separated by centrifugation at 10,000 × *g* for 20 min and filtered through a 0.45 µm cellulose acetate filter. The leached metal ions (iron and molybdenum) were measured using inductively coupled plasma optical emission spectroscopy (ICP-OES, iCAP 7000 series, Thermo Scientific, USA). All experiments were performed in triplicate, and the mean values were calculated.

Results and Discussion

Biosynthesis of Iron–Molybdenum Bimetallic Nanoparticles

In this study, *Deinococcus radiodurans* was chosen as a host strain for the green synthesis of iron-based nanoparticles because it could efficiently mineralize metal ions into nanoparticles through various metabolites including carotenoids, pyrroloquinoline quinone, and Mn^{2+}-complex molecules [14]. Moreover, this bacterium has remarkable resistance and scavenging ability to strong oxidant, hydrogen peroxide (H_2O_2), which is a trigger molecule to initiate the Fenton reaction [15]. Molybdenum is recognized as an effective co-catalyst in the Fenton reaction due to its ability to enhance the generation of hydroxyl radicals (•OH), which are the crucial species responsible for oxidation of contaminants [16, 17]. Therefore, molybdenum (Mo) was also selected as a component of biogenic bimetallic nanoparticles along with iron (Fe). First, the bimetallic FeMoNPs were synthesized in vivo using the *Deinococcus radiodurans* R1 strain cultured with TGY medium supplemented with Na_2MoO_4•$2H_2O$ and $FeCl_3$•$6H_2O$ (a volume ratio of 13:9) for 24 h. During cultivation, the color of cell cultures gradually changed from yellowish to dark brown over time, indicating that the nanoparticles were synthesized in vivo (Fig. 1, top). It was also found that the formation of nanoparticles was gradually accelerated during 9 h incubation period, almost reaching maturation within 24 h (Fig. 1, bottom).

An SEM–EDX analysis was performed to determine the morphology and elemental composition of biogenic FeMoNPs. The biogenic FeMoNPs were not only spherical and had an irregular shape but also contained Fe (0.7 and 6.43 keV) and Mo (2.3 keV) (Fig. 2a–c). These results demonstrated that bimetallic FeMoNPs were successfully

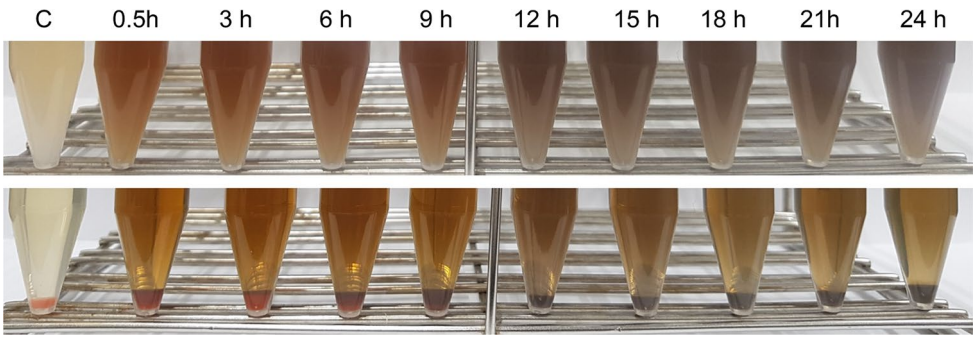

Fig. 1 The formation of iron–molybdenum nanoparticles (FeMoNPs) mediated by *D. radiodurans* R1 strain during 24 h incubation. Top and bottom panels indicate *D. radiodurans* cultures treated with 9.389 mM Na_2MoO_4•$2H_2O$ and 6.5 mM $FeCl_3$•$6H_2O$ at each timepoint before and after centrifugation, respectively. *C* control sample before treatment of metal substrates

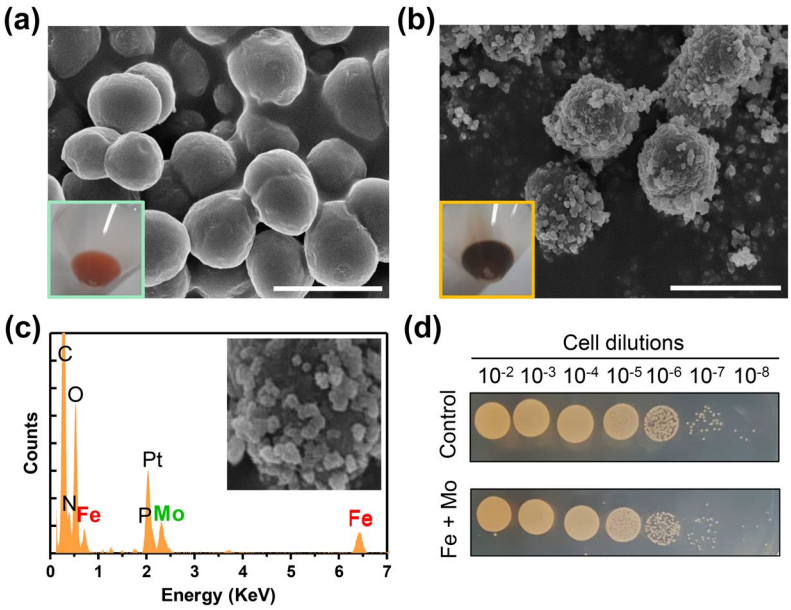

Fig. 2 Scanning electron microscopy images of **a** wild-type *D. radiodurans* (DR) R1 and **b** iron–molybdenum nanoparticles (FeMoNPs) immobilized *D. radiodurans* R1 strain (DR-FeMoNPs) at X 50 k magnification (scale bar = 2 µm). **c** Energy-dispersive X-ray spectrometry spectrum on the surface of DR-FeMoNPs (inset image indicates EDX scanning area). **d** Cell viability of *D. radiodurans* R1 after biosynthesis of FeMoNPs

synthesized in vivo and immobilized onto the *D. radiodurans* R1 strain. Furthermore, in contrast to prior studies that reported the cytotoxicity of nanoparticles, no growth retardation was observed during the synthesis of FeMoNPs (Fig. 2d). Interestingly, during the EDX analysis, the peaks corresponding to elements C, O, N, and P were also analyzed. This is possibly due to the presence of biomolecules, such as proteins and exopolysaccharides, constituting the cell membrane of live *D. radiodurans* R1 [18, 19]. These surface biomolecules are associated with adsorption and maturation of nanoparticles. There have been several previous studies reporting the crucial biological factors for green synthesis of nanoparticles in *D. radiodurans*. Li et al. reported that some functional groups such as hydroxyl, amine, and phosphate on the *D. radiodurans* cell surface played an important role in the reduction and stabilization of gold nanoparticles (AuNPs) [19]. Notably, the membrane-associated deinoxanthin played as a reducing molecule in the biotransformation process of gold ions [Au(III)] into AuNPs [20, 21]. The immobilization of nanoparticles onto the cell surface is also mainly due to the presence of S-layer proteins located in surface area of *D. radiodurans* [22].

Analysis of Biogenic Iron–Molybdenum Nanoparticles

The physicochemical properties of nanomaterials are dictated by their dimensions, including size and surface area. To investigate the surface chemistry of in vivo-synthesized FeMoNPs, Dynamic Light Scattering (DLS), X-ray diffraction (XRD), and X-ray photoelectron spectroscopy (XPS) analyses were performed [23]. As observed in Fig. 3a, b, the size distribution of biological FeMoNPs primarily ranged from 58.7 nm to 68.0 nm. Additionally, broad shoulder peaks indicative of organic matter-related biotransformation were identified in the range of 20° to 30° 2θ [19, 24, 25]. These results indicated that FeMoNPs synthesized by live *D. radiodurans* R1 strain have an amorphous structure like other biologically synthesized nanoparticles. A similar pattern in the biogenic nanoparticle is also observed in a previous study reporting the development of an arsenic treatment method using live-cell fabricated iron nanoparticles [12].

In the XPS analysis, all binding energy (eV) peaks calibrated to the adventitious C 1 s peak at 284.8 eV were observed as 1 s, N 1 s, P 1 s, O 1 s, Fe 2p, and Mo 3d (Fig. 3c). The core-level spectra of C 1 s, N 1 s, and P 1 s identified the functional groups of *D. radiodurans* R1 involved in forming the nanoparticles [18]. The peaks at 724.9 eV and 711.1 eV for Fe^{3+} were assigned to Fe $2p_{1/2}$ and Fe $2p_{3/2}$, respectively. The Mo $3d_{3/2}$ and Mo$3d_{5/2}$ peaks for Mo^{6+} appeared at 235.4 eV and 232.2 eV, and the O 1 s peak at 531.2 eV indicated oxygen from the metal oxides. These results correlate with a previous study reporting the characterization of ferrimolybdite nanowires [13].

Next, the Brunauer–Emmett–Teller (BET) and Barrett–Joyner–Halenda (BJH) analyses were also performed to investigate the specific surface area and porosity of FeMoNPs. According to the International Union of Pure and Applied Chemistry classification system, the FeMoNPs exhibited type IV isotherms with type H3 hysteresis loop characteristics with a mesoporous system (Fig. 4a). An H3 hysteresis loop indicated that the pores were interconnected and randomly distributed [26]. Moreover, a thin hysteresis loop formed between a relative pressure (P/P_0) of 0.85 and 0.95 indicated that FeMoNPs have both meso- and macropores [27]. As illustrated in Fig. 4b, the FeMoNPs exhibited

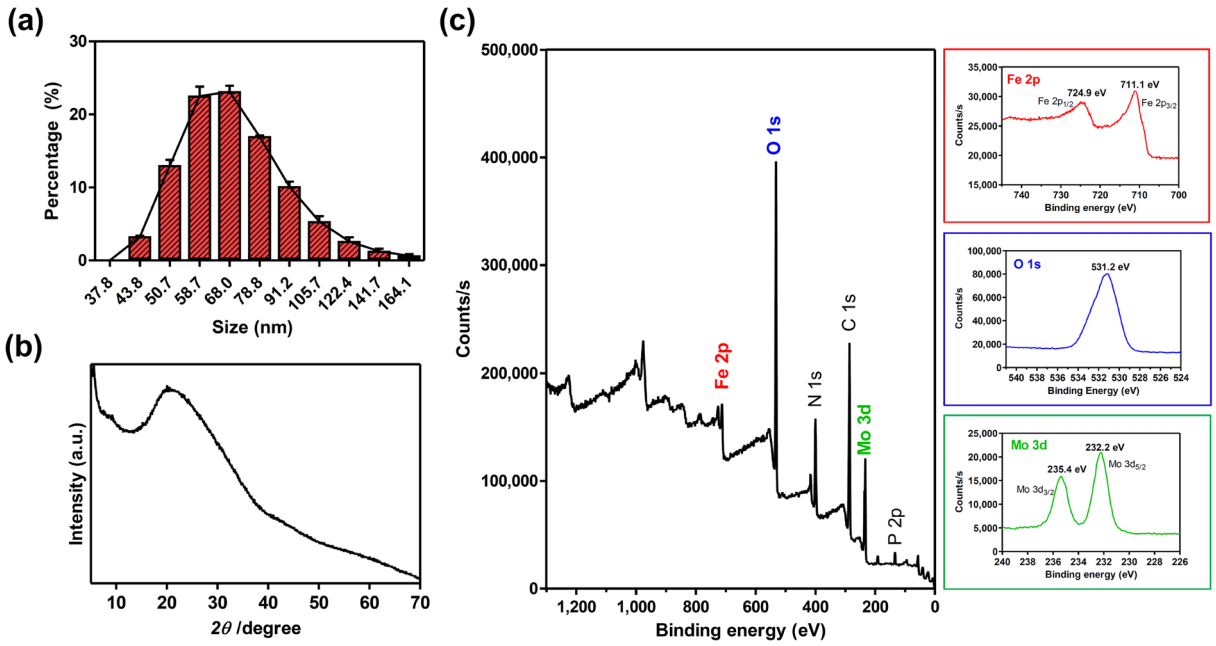

Fig. 3 Characterization of the biogenic iron–molybdenum nanoparticles (FeMoNPs). **a** Size distribution, **b** X-ray diffraction patterns, and **c** X-ray photoelectron spectroscopy (XPS) spectra. Each XPS spectrum for Fe 2p, O 1 s, and Mo 3d shows enlarged images in the right panels

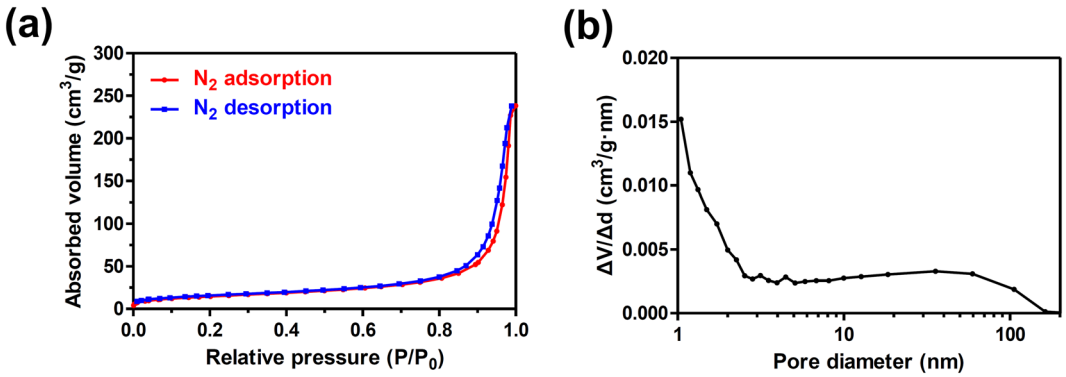

Fig. 4 Brunauer–Emmett–Teller (BET) and Barret–Joyner–Halenda (BJH) analyses of iron–molybdenum nanoparticles (FeMoNPs). **a** Nitrogen adsorption–desorption isotherms and **b** the corresponding pore-size distribution curve of FeMoNPs

two pore-size distributions in the mesoporous and macroporous regions: one with a relatively narrow pore-size distribution in the range of 1 to 9.96 nm and the other with a broad size distribution centered at 57.48 nm. The specific surface area, pore volume, and average pore diameter of FeMoNPs obtained by the BET and BJH analyses were 53.627 $m^2\ g^{-1}$, 0.3561 $cm^3\ g^{-1}$, and 19.205 nm, respectively.

Based on these results, the biogenic FeMoNPs developed here exhibited a larger surface area compared to chemically synthesized nanoparticles, such as Al-doped zinc oxide (34.3 $m^2\ g^{-1}$), porous ZnO nanosheets (12.5 $m^2\ g^{-1}$), and 3D nanoporous Cu (6.0 $m^2\ g^{-1}$) [27, 28]. Therefore, FeMoNPs synthesized in vivo can be expected to be functional and effective compared to nanoparticles used in conventional processing methods.

Treatment of Congo Red Using DR-FeMoNPs

Next, to investigate the removal capability of FeMoNPs-immobilized *D. radiodurans* R1 strain (DR-FeMoNPs) on azo compounds, the treatment of aqueous media contaminated with Congo Red was conducted. To establish the optimal H_2O_2 concentration, an analysis of the decomposition efficiency of Congo Red based on varying H_2O_2 concentrations was conducted. As shown in Fig. 5a, the removal efficiency exhibited a rapid increase up to an H_2O_2

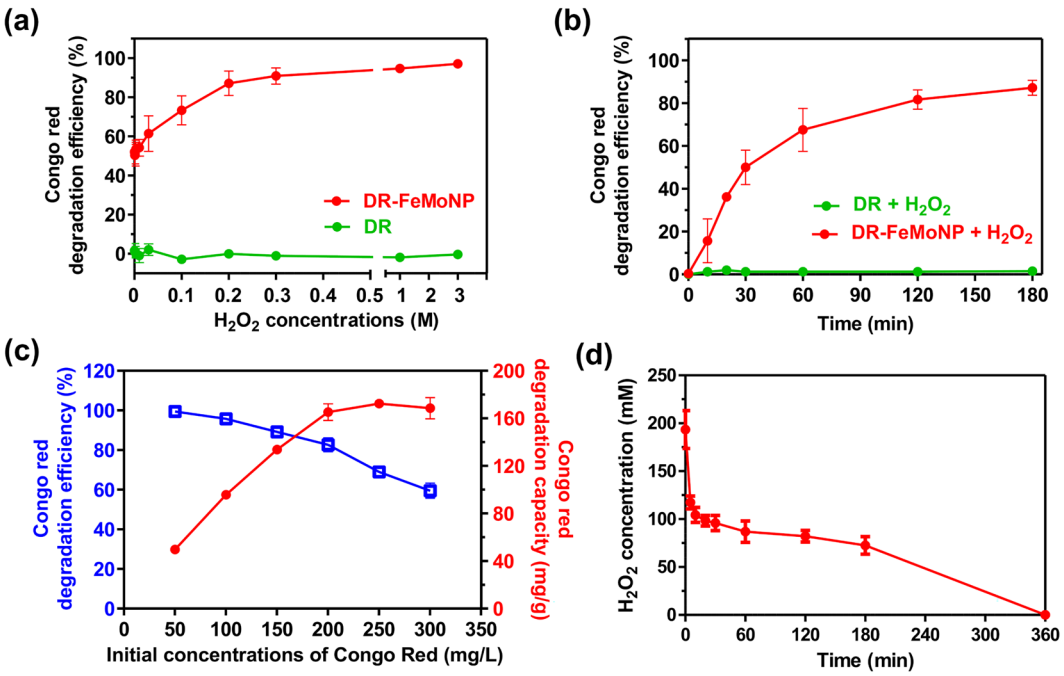

Fig. 5 Degradation of Congo red via the Fenton-like reaction using DR-FeMoNPs and the optimization process. **a** Effect of H_2O_2 concentration on the degradation efficiency for Congo red (200 mg/L) on 1 g/L of DR-FeMoNPs for 3 h. **b** Effect of reaction time on the degradation efficiency for Congo red (200 mg/L) by DR-FeMoNPs (1 g/L) and H_2O_2 (0.2 M). *D. radiodurans* (DR) cells were used as the control. **c** Congo red degradation efficiency and capacity of DR-FeMoNPs at different initial Congo red concentrations (1 g/L of DR-FeMoNPs, 0.2 M H_2O_2, and incubation for 3 h). **d** Time-course analysis of H_2O_2 decomposition during microbial Fenton-like reaction. Experiments were carried out in triplicate, and the error bars indicate the standard deviation

concentration of 0.2 M and then tended to remain constant thereafter. Therefore, a concentration of 0.2 M H_2O_2 was selected as the optimal condition for treating water contaminated with azo dye. As depicted in Fig. 5b, DR-FeMoNPs exhibit rapid Congo Red degradation kinetics at an early stage. More than 50% of the Congo red was rapidly removed by DR-FeMoNPs within 30 min. Although the removal efficiency somewhat gradually decreased as the reaction proceeded to equilibrium status, DR-FeMoNPs showed 87.2% degradation efficiency at the end of the reaction (180 min). Besides, the maximum degradation efficiency (99.5%) and the maximum degradation capacity (172.4 mg/g) of the DR-FeMoNPs were also observed at 50 mg/L and 250 mg/L of initial Congo red concentrations, respectively (Fig. 5c). The mechanism of Congo red degradation through Fenton-like system can be described by Eqs. (3)-(6). In this reaction, Fe^{3+} and MoO_4^{2-} primarily reacted with H_2O_2 to form Fe^{2+}, MoO_4^{3-}, and $HO_2^{\cdot}$ radical [Eq. (3)] [29, 30]. The reduced Fe^{2+} and MoO_4^{3-} ions can also react with H_2O_2 to generate Fe^{3+}, MoO_4^{2-}, OH^-, and $^{\cdot}OH$ radical [Eq. (4)] [31]. The $HO_2^{\cdot}$ can be further converted into its conjugation base, $O_2^{-\cdot}$ [Eq. (5)] [32]. Both $^{\cdot}OH$ and $O_2^{-\cdot}$ radicals generated from Fenton-like reaction are capable of degrading Congo red into non-toxic oxidized products [Eq. (6)].

$$Fe^{3+} + MoO_4^{2-} + H_2O_2 \rightarrow Fe^{2+} + MoO_4^{3-} + 2HO_2^{\cdot} + 2H^+ \quad (3)$$

$$Fe^{2+} + MoO_4^{3-} + H_2O_2 \rightarrow Fe^{2+} + MoO_4^{3-} + 2^{\cdot}OH + 2OH^- \quad (4)$$

$$HO_2^{\cdot} \leftrightarrow H^+ + O_2^{-\cdot} \quad (5)$$

$$^{\cdot}OH + O_2^{-\cdot} + \text{Congo Red} \rightarrow \text{oxidized products} \quad (6)$$

It was interesting to note that H_2O_2 decomposed rapidly for up to 20 min, and the residual H_2O_2 was completely decomposed within 360 min (Fig. 5d). The additional decomposition of H_2O_2 is presumed to be attributed to the *D. radiodurans* strain used in this study. This bacterium could immediately respond to external H_2O_2 stress by inducing strong antioxidant enzymes such as catalases, peroxidases, and superoxide dismutases. This is the notable advance of this study with the aid of its excellent scavenging activity against reactive oxygen species (ROS) [33]. Thus, the DR-FeMoNPs-mediated microbial Fenton-like reaction developed here has great potential not only for the treatment of azo compounds contaminated aqueous

media, but also to solve critical problems for secondary contamination caused by excessive residual H_2O_2.

Stability and Reusability of the DR-FeMoNPs

When utilizing nanoparticles for the purpose of environmental treatment, the investigation of their metal leaching properties is essential to ensure the effectiveness of the remediation process and prevent the generation of secondary contaminants. As can be seen in Fig. 6a, only 6.1 mg/L of Fe and 44.7 mg/L of Mo ions were released during the reaction. This is relatively lower than those reported in previous studies reporting the metal leaching properties of chemically synthesized nanoparticles. In a prior study, approximately 21.5 mg/L of Fe and 78.8 mg/L of Mo were released from 1 g/L of chemically synthesized ferrimolybdite nanowires used in the treatment of Congo Red [13]. Another study also reported that approximately 5.1% of total Fe (12.2 mg/L) was released from heterogeneous ferrite nanoparticles applied for the treatment of Rhodamine B [34]. Additionally, the developed DR-FeMoNPs exhibited a treatment efficiency of approximately 80% for up to two reuses; however, when reused more than three times, the treatment efficiency for azo compounds decreased by more than 38% (Fig. 6b). The decrease in Congo red removal efficiency during repeated reaction process might be caused by the leached metal ions from the FeMoNPs, agglomeration of nanoparticles, and accumulation of by-products, which could inhibit the active sites on the catalysts [35–37]. This outcome represents a notable advantage of DR-FeMoNPs, indicating that the method developed in this study has promise as a sustainability and eco-friendly treatment approach compared to the currently used conventional physicochemical treatment methods.

Application of DR-FeMoNPs on Treatment of Other Azo Dyes

Additionally, to see if the microbial Fenton-like reaction using DR-FeMoNPs is also effective in the treatment of other azo dyes, removal efficiency of Acid orange 7 and Evans blue was investigated. As can be seen in Fig. 7, the DR-FeMoNPs showed more than 81.1% (removed from 100.63 mg/L to 18.93 mg/L) and 99.4% (removed from 99.36 mg/L to 0.63 mg/L) of removal efficiency in the treatment of Acid orange 7 and Evans blue, respectively.

Over the past few decades, numerous studies have investigated on environmental treatment of toxic pollutants using chemically synthesized nanoparticles, which offer several advantages such as high reactivity and efficiency [7, 8]. However, there are still drawbacks and challenges, including

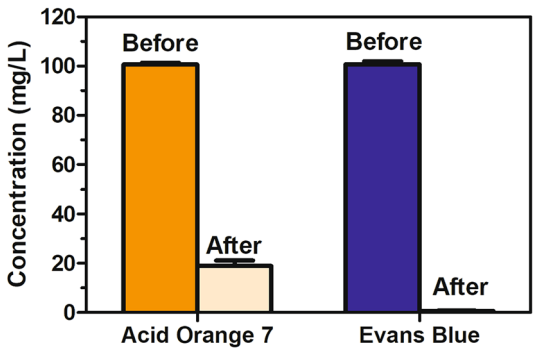

Fig. 7 Degradation of Acid Orange 7 and Evans Blue using DR-FeMoNPs. Experimental conditions: 1 g/L of DR-FeMoNPs, 100 mg/L of dye solutions, 0.2 M H_2O_2, and 3 h reaction time. Experiments were carried out in triplicate and the error bars indicate the standard deviation

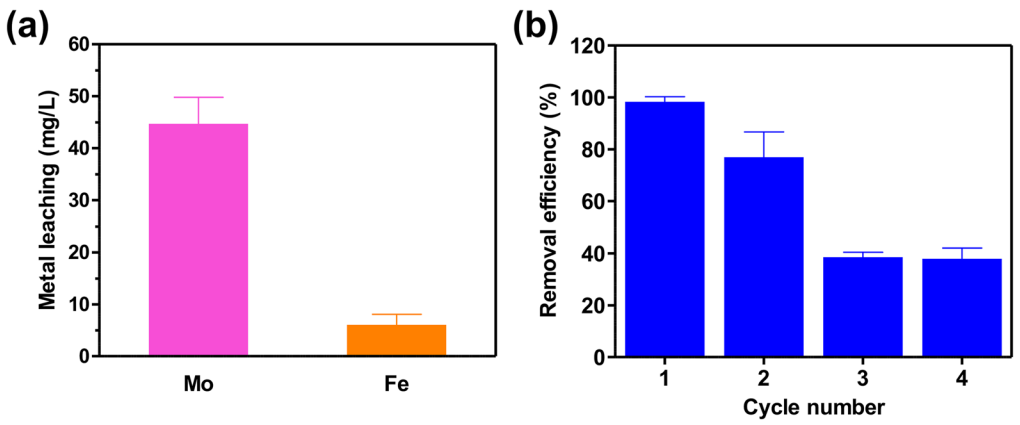

Fig. 6 **a** Iron (Fe) and molybdenum (Mo) leaching after Fenton-like reaction. **b** The changes of Congo red removal efficiency during repeated use. Experimental conditions: 1 g/L of DR-FeMoNPs, 100 mg/L of Congo solution, 0.2 M H_2O_2 and 3 h of reaction time. Experiments were carried out in triplicate and error bars indicate the standard deviation of the mean

cost, scalability, and energy consumption. For example, mass production of target-specific nanoparticles can be expensive, making their versatility and scale-up difficult. Additionally, the synthesis of nanoparticles often requires energy-intensive and environmentally harmful processes. Considering these concerns, an eco-friendly sustainable nanoparticle synthesis method employing living cells emerges as a promising solution to address the existing methods currently used in terms of cost-effectiveness, energy saving, and environmental friendliness. Furthermore, the utilization of living microorganisms in nanoparticle synthesis, coupled with their direct application in environmental treatment, offers the advantage of concurrent biological decomposition alongside nanoparticle-mediated degradation. From the perspective of bioremediation technology, extremophiles also provide numerous advantages. They can adapt to and thrive in extreme environmental conditions beyond the range tolerable by humans, such as high acidity, high temperature, dryness, and cold. This adaptability makes them highly advantageous for the removal of pollutants in extreme environments.

Conclusions

In this study, we successfully developed a highly efficient and reliable azo compounds treatment method by using microorganism immobilized with biogenic nanoparticles. To achieve this, bimetallic iron–molybdenum nanoparticles (FeMoNPs) was successfully synthesized using a live *Deinococcus radiodurans* R1 strain and confirmed the immobilization onto the surface area of the cell (DR-FeMoNPs). The resulting DR-FeMoNPs mediated Fenton-like reaction exhibited 87.2% Congo Red degradation efficiency and 172.4 mg/g of maximum degradation capacity. In addition, the remaining H_2O_2 after the reaction was rapidly decomposed due to the strong ROS scavenging activity of *D. radiodurans* microorganisms. DR-FeMoNPs also showed highly efficient removal efficiency on the treatment of Acid Orange 7 (81.1%) and Evans Blue (99.4%). Furthermore, DR- FeMoNPs exhibited significantly lower metal leaching properties than those of chemically synthesized nanoparticles. All things taken together, the DR-FeMoNPs developed here is promising and superior to the currently employed treatment method in terms of sustainability, eco-friendly, and expandability through the biosynthesis of various nanoparticles. If desired, the treatment efficiency and maximum capacity resulting from the biogenic nanomaterials could be upgraded through synthetic biology and bioengineering approaches.

Acknowledgements This work was supported by the Basic Study and Interdisciplinary R&D Foundation Fund of the University of Seoul (2020) for Yong Jun Choi and the National Research Foundation of Korea (NRF) grant funded by Korea government (MSIT) (No. RS-2023-00213102) for Jung Eun Yang.

Data availability All data supporting the findings of this study are available within the paper.

References

1. Y. Zhang, F. Gao, B. Wanjala, Z.Y. Li, G. Cernigliaro, G. Gu, Appl. Catal. B Environ. **199**, 504 (2016)
2. K.T. Chung, J Environ Sci Health Care **34**, 233 (2016)
3. S.Y. Zhu, S.H. Jiao, Z.W. Liu, G.S. Pang, S.H. Feng, Environ. Sci. Nano **1**, 172 (2014)
4. T. Hara, M. Ishikawa, J. Sawada, N. Ichikuni, S. Shimazu, Green Chem. **11**, 2034 (2009)
5. R. Chen, W. Wang, X.R. Zhao, Y.J. Zhang, S.Z. Wu, F. Li, Chem. Eng. J. **242**, 226 (2014)
6. F.F. Chen, X. Wu, R. Bu, F. Yang, RSC Adv. **7**, 41945 (2017)
7. Z.D. Fang, K. Zhang, J. Liu, J.Y. Fan, Z.W. Zhao, Water Sci Eng **10**, 326 (2017)
8. M.I. Litter, M. Slodowicz, J Adv Oxid Technol **20**, 0164 (2017)
9. J.A. Zazo, G. Pliego, S. Blasco, J.A. Casas, J.J. Rodriguez, Ind. Eng. Chem. Res. **50**, 866 (2011)
10. F. Büyüksönmez, T.F. Hess, R.L. Crawford, R.J. Watts, Appl. Environ. Microbiol. **64**, 3759 (1998)
11. M.H. Choi, S.-W. Jeong, H.E. Shim, S.-J. Yun, S. Mushtaq, D.S. Choi, B.-S. Jang, E.Y. Yang, Y.J. Choi, J.H. Jeon, Chem. Commun. **53**, 3937 (2017)
12. H.K. Kim, S.-W. Jeong, J.E. Yang, Y.J. Choi, Int. J. Mol. Sci. **20**, 3566 (2019)
13. Y.C. Su, W. Luo, L. Zhang, C. Bao, P. Sun, N. Huang, Y. Sun, L. Fang, L. Wang, Environ. Sci. Nano **5**, 2069 (2018)
14. X. Anqi, W. Bixuan, Z. Liying, J. Ling, Process Biochem. **100**, 217–333 (2021)
15. F. Liu, N. Li, Y. Zhang, Radiat Med Prot **4**, 70–79 (2023)
16. J. Ji, Y. Bao, X. Liu, J. Zhang, M. Xing, EcoMat **3**, e12155 (2021)
17. W. Qin, Y. Ma, T. He, J. Hu, P. Gao, S. Yang, Nanomaterials **12**, 4138 (2022)
18. R.R. Kulkarni, N.S. Shaiwale, D.N. Deobagkar, D.D. Deobagkar, Int. J. Nanomed. **10**, 963 (2015)
19. J.L. Li, Q. Li, X. Ma, B. Tian, T. Li, J. Yu, S. Dai, Y. Weng, Y. Hua, In. J Nanomed **11**, 5931 (2016)
20. B. Tian, J. Li, R. Pang, D. Shang, T. Li, Y. Wang, Y. Hua, A.C.S. Appl, Mater Interfaces **10**, 37353 (2018)
21. A. Chen, L.M. Contreas, B.K. Keitz, Appl. Environ. Microbiol. **83**, e00798 (2017)
22. J. Li, B. Tian, T. Li, S. Dai, Y. Weng, J. Lu, X. Xu, Y. Jin, R. Pang, Y. Hua, Int. J. Nanomed. **13**, 1411 (2018)
23. Z.Q. Cai, Y.M. Sun, W. Liu, F. Pan, P.Z. Sun, J. Fu, Environ. Sci. Pollut. Res. **24**, 15882 (2017)
24. S.V. Liu, J. Zhou, C. Zhang, D.R. Cole, M. Gajadarziska-Josifovska, T.J. Phelps, Science **277**, 1106 (1997)
25. Y. Roh, R.J. Lauf, A.D. Millan, C. Zhang, C.J. Rawn, J. Bai, T.J. Phelps, Solid State Commun. **118**, 529 (2001)
26. C. Santhosh, P. Kollu, S. Felix, V. Velmurugan, S.K. Jeong, A.N. Grace, RSC Adv. **5**, 28965 (2015)
27. X. Sun, W. Luo, L. Zheng, C. Bao, P. Sun, N. Huang, Y. Sun, L. Fang, L. Wang, RSC Adv. **6**, 2241 (2016)
28. C. Yang, C. Zhang, L. Liu, J Mater Chem A **42**, 20992 (2018)
29. I. Popivker, I. Zilbermann, E. Maimon, H. Cohen, D. Meyerstein, Dalton Trans. **42**, 16666–16668 (2013)
30. S.H. Tian, Y.T. Tu, D.S. Chen, X. Chen, Y. Xiong, Chem. Eng. J. **169**, 31–37 (2011)
31. X.Q. Fan, H.Y. Hao, Y.C. Wang, F. Chen, J.L. Zhang, Environ. Sci. Pollut. Res. **20**, 3649–3656 (2013)

32. H.Y. Zhao, Y.J. Wang, Y.B. Wang, T.C. Cao, G.H. Zhao, Appl. Catal. B **125**, 120–127 (2012)
33. D. Slade, M. Radman, Microbiol Mol Biol Rev **75**, 133 (2011)
34. T.R. Giraldi, C.C. Arruda, G.M. da Coasta, E. Longo, C. Ribeiro, J. Sol-Gel, Sci Technol **52**, 299 (2009)
35. C. Wang, R. Jiang, J. Yang, P. Wang, Front. Chem. **10**, 892424 (2022)
36. Z. Liu, X. Ge, Y. Wang, S. Jiang, S. Sun, Colloids Surf A Physicochem Eng **684**, 133135 (2024)
37. G. Ren, K. Zhao, L. Zhao, RSC Adv. **10**, 39973–39980 (2020)

Publisher's Note Springer Nature remains neutral with regard to jurisdictional claims in published maps and institutional affiliations.

Springer Nature or its licensor (e.g. a society or other partner) holds exclusive rights to this article under a publishing agreement with the author(s) or other rightsholder(s); author self-archiving of the accepted manuscript version of this article is solely governed by the terms of such publishing agreement and applicable law.